FULL PAPER

WILEY Applied Organometallic Chemistry

Rapid Suzuki-Miyaura cross-coupling reaction catalyzed by zirconium carboxyphosphonate supported mixed valent Pd(0)/Pd(II) catalyst

Bagmita Bhattacharyya[1] | Jyoti Prasad Biswas[1] | Shashank Mishra[2] (iD) | Nayanmoni Gogoi[1] (iD)

[1] Department of Chemical Sciences, Tezpur University, Napaam 784028 Sonitpur, Assam, India

[2] Institut de recherches sur la catalyse et l'environnement de Lyon, Université Claude Bernerd Lyon 1, IRCELYON, CNRS-UMR 5256, 2 Avenue Albert Einstein, 69626 Villeurbanne, France

Correspondence
Nayanmoni Gogoi, Department of Chemical Sciences, Tezpur University, Napaam, 784028, Sonitpur. Assam, India.
Email: ngogoi@tezu.ernet.in

Mixed valent Pd(0)/Pd(II) nano-sized aggregates supported onto a chemically robust layered zirconium carboxyphosphonate framework is prepared and its catalytic activity in Suzuki-Miyaura cross coupling reaction is explored. The exceptionally high catalytic efficacy of the heterogeneous catalyst in Suzuki-Miyaura cross coupling reaction is signified by remarkably short reaction time 2 minutes and high turnover frequency of 1.3×10^4 hr^{-1}. The catalyst can be recycled several times without significant loss of catalytic efficacy, while spectroscopic, structural and microscopic investigations suggest the integrity of the catalyst even after fifth catalytic cycle. The unique ability of the zirconium carboxyphosphonate framework to interact strongly with palladium in dual Pd(0)/Pd(II) oxidation states has been attributed to this remarkable augmentation of catalytic efficacy.

KEYWORDS
heterogeneous catalysis, layered zirconium carboxyphosphonate, Pd(0)/Pd(II) nanoaggregate

1 | INTRODUCTION

Enhancing the efficiency of heterogeneous catalysts to match their homogeneous counterparts has emerged as one of the most pressing challenge for furthering their industrial applications.[1–3] Current outbursts of activities to address this concern primarily relies on tuning the surface area and electronic characteristics of active catalytic species either by particle size miniaturization or by manipulating interaction with support surface.[4–6] In this regard, development of highly reactive heterogeneous palladium-based catalysts for cross coupling reactions are of particular interest due to their relevance as indispensable synthetic tools for chemist.[7,8] Concern over limited catalyst reusability and contamination of residual palladium in products led to the proliferation of heterogeneous catalysts for these cross coupling reactions. A fascinating assortment of highly efficient heterogeneous catalyst, prepared by immobilization of palladium nanoparticles over a wide array of solid supports, e.g., carbon based materials,[9] silicious materials,[10] polymers,[11] metal–organic frameworks[12,13] have already been reported. Many of these heterogeneous catalysts can be easily recycled and repeatedly used, afford products in high yields within a reasonably short reaction time, require mild reaction conditions in green solvent medium or even under solventless conditions. Nonetheless, in terms of catalyst reactivity, majority of reported heterogeneous catalysts fare quite poorly as compared to their homogeneous counterparts and this attribute primarily manifests itself as typically longer reaction completion time when heterogeneous catalyst are employed.[14] For example, in case of Suzuki-Miyaura cross coupling reaction of aryl bromides with aryl boronic acid, reaction completion time of as short as 1–2 mins with concomitantly high turn-over frequency have been reported when adequately reactive homogeneous catalyst are employed.[15–17] However, to the best of our

knowledge, no heterogeneous catalyst which can effect satisfactory conversion in less than 15 mins under conventional heating has been reported so far.[18–21] Thus, development of heterogeneous catalysts whose efficacies in cross coupling reaction are comparable to that of homogenous palladium-based catalysts remains a highly desirable objective.

During this study, a strategy based on both particle size miniaturization and surface functionalization of the catalytically active species by using a suitable solid support has been adopted to enhance the efficacy of heterogeneous catalyst in cross coupling reaction. The solid support chosen for immobilization of palladium nanoparticles is a layered mesoporous zirconium organophosphonate framework decorated with additional L-proline functionality. The L-proline functionalized phosphonate ligand, 1-Phosphonomethyl-pyrrolidine-2-carboxylic acid can be easily synthesized by following literature procedure and it provides an easy access to zirconium organophosphonate framework functionalized with L-proline (Scheme 1).[22] It is anticipated that large surface area and intrinsic chemical robustness of the zirconium organophosphonate framework will facilitate palladium nanoparticle loading and improve reusability of the catalyst, respectively.[23,24] Indeed, mesoporous metal organophosphonates are widely recognized as a versatile class of support materials for metal or metal oxide nanoparticles.[25–28] Recent reports have established the superior ability of amino acid-functionalized zirconium phosphonate frameworks in immobilization of 2–5 nm palladium nanoparticles resulting in high catalytic activity.[29–31] Due to the layered structure of zirconium organophosphonates, the amino acid groups lie over the surface of the solid support in a well ordered fashion which significantly accentuates their ability to interact with substrates immobilized over the framework.[32–34] Furthermore, several homogeneous as well as heterogeneous palladium catalysts bearing L-proline display significantly enhanced reactivity in cross-coupling reactions.[35–39] Therefore, it is expected that immobilized palladium nanoparticles will interact strongly with the L-proline functionality present over the surface of the zirconium organophosphonate framework and thereby augment the reactivity of the catalyst in cross coupling reactions.
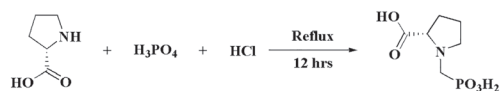
SCHEME 1 Synthesis of 1-Phosphonomethyl-pyrrolidine-2-carboxylic acid

2 | EXPERIMENTAL SECTION

2.1 | Materials and methods

Starting materials were purchased from commercial sources and used without further purification. Solvents were purified by conventional techniques and distilled prior to use. Elemental analyses were performed on a Perkin Elmer Model PR 2400 series II elemental analyzer. Fourier transformed infrared spectra from 400 to 4000 cm^{-1} were recorded on Perkin Elmer Frontier MIR-FIR FT-IR spectrophotometer. ICP-OES analysis was performed using Perkin Elmer Optima 2100 DV Optical Emission Spectroscopy analyzer. Thermogravimetric analysis was performed with the help of Thermal analyzer (Model TGA-50 & DSC-60, Shimadzu). NMR spectra were recorded on a JEOL JNM-ECS400 NMR spectrometer operating at 400 MHz and samples were dissolved in deuterated solvents. Chemical shifts were reported in parts per million downfield of Me$_4$Si (TMS) as internal standard. The scanning electron microscopy (SEM) analyses were carried out using a JEOL JSM-6390LV SEM, equipped with an Energy-Dispersive X-ray analyzer. The powder X-ray diffraction patterns were recorded on a Rigaku Multiflex instrument using a nickel-filtered CuKα (0.15418 nm) radiation source and scintillation counter detector. The surface area and pore size distribution of the compound were analyzed using BET surface analyzer (QUANTACHROME NOVA 1000E). The transmission electron microscopy analyses were carried out using JEM-2100, 200 kV, Jeol instrument. X-ray photoelectron spectroscopic (XPS) analyses were performed in KRATOS Axis ultra DLD spectrometer using Al Kα (1486.6 eV) radiation source. Magic angle spinning NMR (MAS NMR) of ^{13}C and ^{31}P were recorded with AVANCE III 500WB spectrometer using adamantane (δ = 38 ppm) and H$_3$PO$_4$ (δ = 0 ppm) as references, respectively.

2.1.1 | Synthesis of 1-Phosphonomethyl-pyrrolidine-2-carboxylic acid

1-Phosphonomethyl-pyrrolidine-2-carboxylic acid was prepared by following a literature procedure (Scheme 1).[22] To a mixture of L-proline (1.1513 g, 10 mmol), phosphorus acid (0.90 g, 11 mmol) and hydrochloric acid (30 ml), formaldehyde (1.47 ml, 40 mmol) was added dropwise under reflux condition. The resultant mixture was further refluxed for 12 hrs. Thereafter, the resulting solution was evaporated on a water bath to obtain the product as a white solid. Yield:

1.2 g (58%); FT-IR (KBr, cm^{-1}): υ = 3016 (b), 1887(w), 1705 (s), 1452 (vw), 1352 (s), 1250 (s), 1194 (s), 1151 (s), 1078 (s), 1005 (s), 925 (s), 919 (m), 721 (m), 640 (m), 459 (s).; ^{1}H NMR (400 MHz, D$_2$O, δ ppm): 1.87–2.39 (m, 4H), 3.22 (m, 2H), 3.39 (m, 1H), 3.77 (m, 1H), 4.25 (dd, 1H); ^{13}C NMR (100 MHz, D$_2$O, δ ppm): 22.36, 27.78, 50.65, 56.68, 68.91, 171.27(-COOH); ^{31}P NMR (CDCl$_3$, δ ppm): 7.74.

2.1.2 | Synthesis of zirconium carboxyphosphonate (ZrCP)

ZrOCl$_2$.8H$_2$O (322 mg, 1 mmol) was dissolved in water to which CTAB (182 mg, 0.5 mmol) was added and stirred to obtain a clear solution. 1-Phosphonomethyl-pyrrolidine-2-carboxylic acid (104 mg, 1 mmol) was dissolved in 5 mL distilled water and added drop wise to the previous solution. The mixture was then transferred to a Teflon lined container in an autoclave and kept at 130 °C for 3 days. The precipitate obtained was washed several times with distilled water and then refluxed with acidified ethanol for 12 hrs. The residue was then washed several times with ethanol to remove the remaining acid and dried in vacuum at 50 °C. Yield: 177 mg; Elemental analysis % found: C, 11.59%; H, 4.31%; N, 2.04. FTIR (KBr, cm^{-1}): 3408(br), 1734(w), 1621(m, s), 1425(w), 1116(m), 1024(m), 662(w), 475(br, w). TGA (10 °C/min under air): Temperature range (% weight loss): 32–92 °C (17%); 315–390 °C (88%).

2.1.3 | Synthesis of Pd loaded zirconium carboxyphosphonate (Pd@ZrCP)

250 mg of **ZrCP** was taken in a round bottom flask and prepared a suspension of it in THF. A solution of Pd (OAc)$_2$ (50 mg, 2.2 mmol) in THF was taken and added drop wise to the suspension. The mixture was stirred for 12 hrs. The resultant was washed several times with THF and dried under vacuum. 250 mg of the dried product was then dispersed in 10 ml water and ice-cold water solution of NaBH$_4$ (100 mg, 2.6 mmol) was added drop wise to it. The brown color of the compound changed to black immediately. The suspension was further stirred for 3 hrs after which it was washed several times with water and dried under vacuum. FT-IR (KBr, cm^{-1}): 3383(br), 1625(m, s), 1408(w), 1069(m), 1012(m) 658(w), 464(s, w). Pd loading over the **ZrCP** is calculated to be 9.5% from ICP-OES analysis.

2.1.4 | Typical procedure for Suzuki-Miyaura cross-coupling reaction

0.24 mmol of the aryl boronic acid and 0.2 mmol of aryl bromide were dissolved in 12 ml ethanol water (3:1) mixture. To the above solution, 0.25 mmol of potassium carbonate and 0.5 mg (0.22 mol%) of the catalyst was added and the reaction mixture was refluxed in a preheated water bath for 2–10 minutes. The progress of the reaction was monitored by using thin layer chromatography. After completion of the reaction, the catalyst was removed by filtration and ethanol was removed from the filtrate under reduced pressure. The product was extracted from the filtrate by using ethyl acetate and dried over Na$_2$SO$_4$. Yields were determined from GC–MS by using toluene as the internal standard. To investigate the role of the solvents and the base used in the reaction mixture, tests have been carried out using different solvents and bases. It has been found that the use of 3:1 proportion of C$_2$H$_5$OH:H$_2$O system and K$_2$CO$_3$ as base under reflux condition gives the maximum yield in minimum time.

2.1.5 | Catalyst recyclability test

p-Bromo toluene (0.2 mmol) along with phenyl boronic acid (0.24 mmol) under 3:1 C$_2$H$_5$OH: H$_2$O solution at 80 °C in presence of 0.25 mmol of K$_2$CO$_3$ and 0.22 mol% of catalyst **Pd@ZrCP** was taken as a model reaction for determination of the catalytic activity and the recyclability of the catalyst. Reaction time was fixed to 2 minutes for all the catalytic cycles. The reaction time was monitored using a stopwatch and as soon as the time completed the mixture was immediately filtered and the filtered was further centrifuged to ensure no solid catalyst remain in the solution. After that the catalyst was washed with ethanol water solution for 4 times and then the recovered catalyst was used directly for the reaction using same quantity of starting reactants. The catalyst was recycled upto 5 cycles. The reaction was monitored using TLC and further verified by using GC–MS.

2.1.6 | Palladium leaching test

To investigate the leaching of the catalyst in the reaction medium, initially 4-bromotoluene and phenyl boronic acid was used as reactant in 3:1 C$_2$H$_5$OH:H$_2$O solution using 0.5 mg of the catalyst at 80 °C. As the reaction, complete within 2 minutes, the reaction mixture was immediately filtered through a Whatman filter paper under hot condition which was followed by centrifugation to ensure the complete removal of any solid catalyst. Then to the reaction mixture equivalent amount of

4-nitro bromo benzene, phenyl boronic acid and K₂CO₃ were added and reaction was monitored using TLC. No new product has been observed after 2 h of reflux under the same reaction conditions. It was further stirred for another 4 hrs to ensure absence of any product formation.

The possibility of Pd leaching into the reaction mixture was further analyzed with ICP-OES analysis. During standard heterogeneous Suzuki–Miyaura reactions of 4-bromotoluene with phenyl boronic acid, 2 ml of mother liquor was collected by using a syringe filter (Whatman Puradisc 4, 4 mm diameter, 0.45 μm, PTFE) and the solvent was evaporated under reduced pressure. The residue was dissolved in HNO_3 and analyzed by using ICP-OES which showed that concentration of Pd in reaction solution was less than the detection limit (i.e., 50 ppb). The sample collected after the completion of the reaction also shows concentration of Pd in reaction solution below the detection limit.

2.1.7 | Three phase test

Initially, aminopropyl-modified Silica (SiO_2-$C_3H_6NH_2$) was prepared by slight modification of a reported procedure.[40] To a suspension of SiO_2 (100–200 mesh size, 3 g) in dry toluene a solution of 3-Aminopropyl-trimethoxysilane (APTMS) (4.8 ml, 27 mmol) and pyridine (3 ml, 36.9 mmol) were added dropwise through a dropping funnel under N_2 atmosphere. The resulting mixture was refluxed for 24 hrs. After that, the suspension was filtered and Soxhlet extracted with CH_2Cl_2 for another 24 hrs. The resulting solid was dried under vacuum at room temperature to obtain the product as white powder. Yield: 3.25 g; FT-IR: 3448 (b), 2927 (w, b), 1638 (w, b), 1088 (s), 791 (s), 574 (w), 466(s).

For carrying out the three phase test, a procedure developed by Corma et al. was adopted.[41] For this purpose a solid supported aryl bromide was initially prepared A solution of 4-Bromobenzoylchloride (0.800 g, 3.6 mmol) was dissolved in dry THF(10 ml) in a round bottom flask with aminopropyl trimethoxy silane modified silica (SiO_2-$C_3H_6NH_2$) (1 g) and pyridine (404 μL, 5 mmol) under N_2 atmosphere. The mixture was stirred for 12 hrs at 40 °C after which the resulting suspension was filtered and washed 3 times by 20 ml 5% (v/v) HCl in water, followed by 20 ml of 0.2 M aqueous K_2CO_3, 2 washes each with distilled water and with 20 ml of ethanol. The solid was finally washed with large excess of CH_2Cl_2 and finally dried in air. 1.1 g solid is recovered and assigned as BrPhCONHC₃H₆@SiO₂. FT-IR: 3447 (b), 2926 (w, b), 1639 (w, b), 1068 (s), 791 (s), 463 (s).

In the next step, 4-Bromo toluene (0.2 mmol), phenyl boronic acid (0.24 mmol), K_2CO_3 (0.25 mmol) in C_2H_5OH:H_2O (3:1) in presence of catalyst **Pd@ZrCP** (0.5 mg, 0.22 mol%) and BrPhCONH@SiO_2 (200 mg) were refluxed at 80 °C for 2 mins. After this the suspension was analyzed by TLC and the solid was separated under vacuum in hot condition, washed with EtOH and finally extracted with CH_2Cl_2. Another reaction carried out under the same reaction condition but without the addition of 4-bromotoluene to the reaction medium. In this case also the solid was recovered by hot filtration followed by washing with C_2H_5OH, and finally extracted with CH_2Cl_2. The recovered solids from both the reaction mixtures were hydrolyzed with 2 M KOH/H_2O (1.7 g in 10 ml EtOH, 5 ml H_2O) at 90 °C for 3 days. The resulting solution was neutralized with 10% HCl v/v (9.1 ml), extracted with CH_2Cl_2 followed by ethyl acetate, concentrated, and the resulting mixture was analyzed by ^1H NMR.

2.1.8 | Mercury poisoning test

A solution of 4-bromoacetopheneone (0.2 mmol, 34 mg) phenyl boronic acid (0.24 mmol, 29 mg), K_2CO_3 (0.25 mmol, 34 mg) and **Pd@ZrCP** (0.5 mg, 0.22 mol%) was heated at 80 °C for 3 minutes. The progress of the reaction as this point was monitored by TLC & GC–MS. After that metallic mercury (300 equiv) was added to the reaction mixture. The reaction was continued for another 10 minutes under the same reaction condition and the mother liquor was recovered by using a syringe filter (Whatman Puradisc 4, 4 mm diameter, 0.45 μm, PTFE). The recovered solution was concentrated under reduced pressure to remove ethanol, extracted with ethyl acetate and dried over Na_2SO_4 and finally analyzed with GC–MS.[41]

3 | RESULTS AND DISCUSSION

On account of their versatile characteristics, layered mesoporous zirconium carboxy aminophosphonates have found several applications as catalyst support. Herein, we have employed a surfactant assisted sol–gel technique to prepare a mesoporous Zr^{IV} organocarboxyphosphonate, which was subsequently used as a support matrix for palladium mixed valent Pd(0)/Pd(II) nano-sized aggregates. Hydrothermal reaction of ZrOCl₂.8H₂O with 1-Phosphonomethyl-pyrrolidine-2-carboxylic acid in presence of cetyltrimethylammonium bromide (CTAB) at 130 °C for 3 days followed by treatment with ethanolic HCl to remove CTAB, yielded Zr^{IV} organocarboxyphosphonate, **ZrCP** as an off white solid (Scheme 2). Thereafter, the surfactant free Zr^{IV} organocarboxyphosphonate, **ZrCP** was impregnated with Pd(OAc)₂ for a definite period.
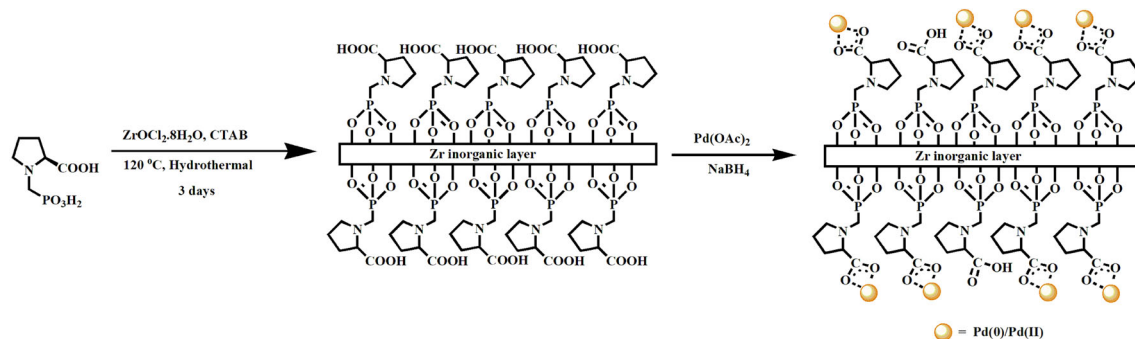
SCHEME 2 Synthesis of ZrCP and Pd@ZrCP

Reduction of absorbed Pd(II) by NaBH$_4$ eventually resulted in palladium incorporated Zr^{IV} carboxyphosphonate composite, **Pd@ZrCP** where Pd(0)/Pd(II) nano-sized aggregates are homogenously dispersed over the Zr^{IV} carboxyphosphonate framework. Both the pristine Zr^{IV} organocarboxyphosphonate, **ZrCP** and the palladium incorporated composite, **Pd@ZrCP** were characterized by various analytical, spectroscopic, microscopic and textural studies such as elemental analysis, FT-IR, MAS NMR, powder X-ray diffraction, SEM, TEM, ICP-OES, XPS, TGA and BET surface area analysis.

All characteristic peaks observed in the FT-IR spectrum of the pristine Zr^{IV} carboxyphosphonate framework, **ZrCP** are also observed in FT-IR spectrum of **Pd@ZrCP** without any significant deviation and this clearly indicates the structural integrity of the host matrix in the composite. IR spectra of both the materials feature an intense and sharp peak at 1024 cm^{-1} which can be attributed to Zr-O-P stretching vibration. Similarly, the peak observed at 1116 cm^{-1} is characteristic of P=O stretching vibration. The intense band observed at ~1625 cm^{-1} can be assigned to C=O stretching vibration associated with the -COOH functionality present within the ligand.[42] Absence of any band near 2260-2340 cm^{-1} region indicates absence of free P-OH groups in the pristine framework as well as the composite. Furthermore, complete removal of CTAB, used for the synthesis of the mesoporous compound is validated by the absence of any peak in the region 2850-2930 cm^{-1} (Figure S1, S2).

Broad peaks observed in the powder X-ray diffraction pattern of both **ZrCP** and **Pd@ZrCP** indicate disordered and amorphous nature of the materials (Figure 1).[43] Furthermore, all peaks observed in the powder X-ray diffraction pattern of **ZrCP** are present in the diffraction pattern of **Pd@ZrCP** and it establishes the integrity of the support within the composite material. Apart from the peaks corresponding to the pristine framework, characteristic peak for (100) plane of metallic palladium is observed at 2θ = 39.4° (JCPDS-87-0641) in the powder X-ray diffraction pattern of **Pd@ZrCP**.
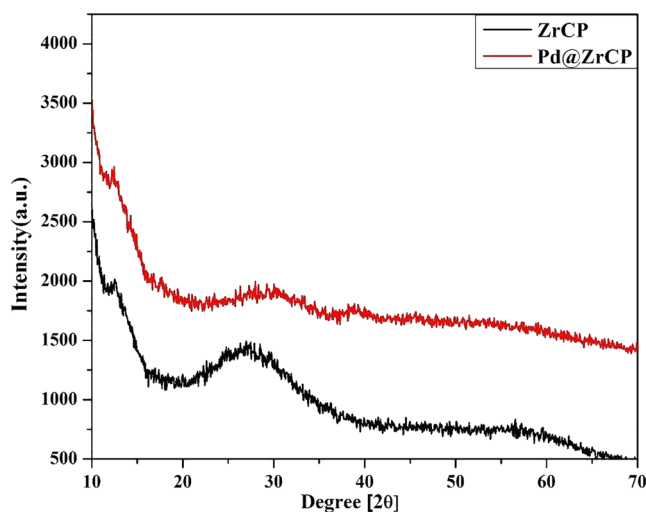
FIGURE 1 Powder X-ray diffraction pattern of ZrCP and Pd@ZrCP

Thermogravimetric analysis of both the pristine framework, **ZrCP** and the composite **Pd@ZrCP** showed rapid weight loss when heated up to 95 °C and this can be attributed to the desorption of water molecules occluded within the host. On heating beyond 100 °C, a gradual weight loss is observed upto 450 °C for both **ZrCP** and **Pd@ZrCP** and this can be attributed to the loss of coordinated water molecules as well as the decomposition of the organic substituents (Figure S3).

Solid state magic angle spinning (MAS) ^{13}C and ^{31}P NMR spectra of both the pristine framework, **ZrCP** and its composite **Pd@ZrCP** were recorded to probe the interaction between immobilized palladium nanoparticles with the solid support. ^{13}C MAS NMR spectra of the **ZrCP** show characteristic peaks for all the carbon atoms of the amino carboxyphosphonate ligand. Peaks observed at 24.1 and 29.4 ppm can be, respectively, assigned to γ- and β-carbon atoms of the pyrrolidine ring. The α- and δ-carbon atoms of pyrrolidine ring resonate at 70.9 and 61.3 ppm, respectively. Signals for the methylene carbon atom attached to phosphonate group and that of the carboxyl carbon atom appear at 52.9 and 173.1 ppm,

respectively (Figure 2). ^{13}C MAS NMR spectrum of **Pd@ZrCP** showed significant variation in the spectral region corresponding to the carboxyl carbon atom of the phosphonate ligand. Unlike to pristine framework, the carboxyl carbon atom in **Pd@ZrCP** resonates as an intense signal centered at 180.0 ppm with two weak shoulders at 172.9 and 188.0 ppm. While the peak at 172.9 can be associated to carboxyl carbon peak observed in the pristine framework, peaks at 180.0 and 188.0 ppm
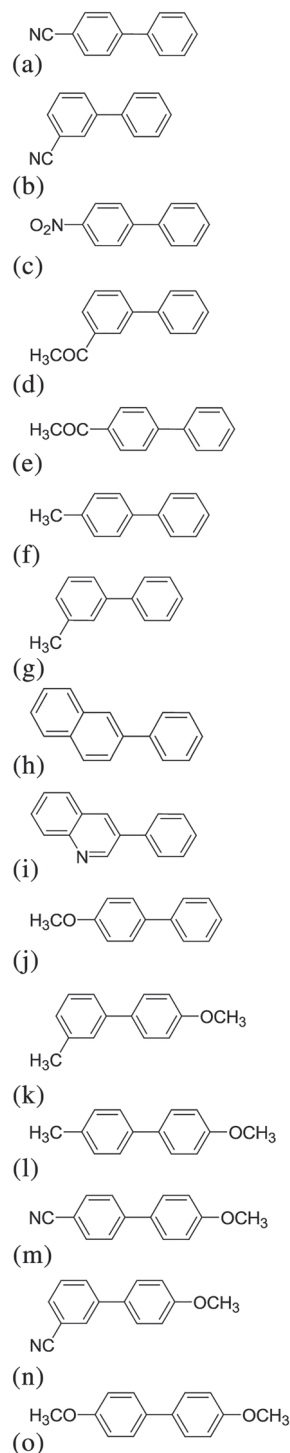

FIGURE 2 ^{13}C MAS NMR spectrum of ZrCP

can be attributed to carboxyl groups having moderate to strong interaction with immobilized palladium nanoparticles (Figure 3). The higher intensity of the peak at 180.0 ppm suggests that majority of the carboxyl group in **Pd@ZrCP** lies at relatively close proximity to the palladium nanoparticles while a small fraction of the carboxyl group remain free from any interaction with embedded nanoparticles. ^{31}P MAS NMR spectra of **ZrCP** shows one broad peak centered at 4.0 ppm and this can be easily assigned to the phosphorous atom of 1-phosphonomethylproline (Figure S11). Loading Pd nanoparticles onto **ZrCP** does not trigger any significant deviation in the chemical shift of phosphorous as the corresponding peak is observed at 4.2 ppm (Figure S12).[33]

The surface morphology of both the pristine framework and its palladium nanocomposite was studied using scanning electron microscopy (SEM). SEM images show presence of micrometer size disordered amorphous particles in both **ZrCP** and **Pd@ZrCP** and surface morphology of the pristine framework does not change after loading palladium nanoparticles (Figure 4). Elemental mapping of **Pd@ZrCP** shows the presence of palladium on the surface of the framework (Figure S4). EDX spectrum shows the presence of Pd in the framework with a percentage loading of 8.5% (Figure S5). EDS mapping show the uniform distribution of palladium over the surface in **Pd@ZrCP** (Figure S4(a) & (b)). From the ICP-OES, it was found that the amount of loading of Pd is about 9.5% (0.89 mmol Pd/g) which is also in agreement with the value found in the surface EDS analysis. The high loading of palladium in **ZrCP** as compared to those reported for other metal organophosphonate support can be attributed to the presence of dangling free carboxylate groups of L-proline groups on the surface of the **ZrCP**, which strongly interact with the embedded metal nanoparticles.[27,28]

TEM images (Figure 5) of **Pd@ZrCP** show palladium nanoparticles of average size 5 nm are homogeneously distributed over the zirconium carboxyphosphonate framework (Figure S13). The selected area electron diffraction (SAED) pattern shows the (100), (200), (222), and (311) planes which corresponds to the fcc structure of the metallic palladium (Figure S6). The N_2 absorption/desorption isotherm of **ZrCP** show hysteresis loop and a sudden jump at $P/P_0 = 0.90$ and this can be mainly attributed to the layered structure. Moreover, the BJH pore size analysis of the pristine framework revealed that the BJH pore volume is 0.893 cc/g and pore radius is 11.0 nm and this establish the mesoporous character of the solid support. BET surface area analysis reveals that of **ZrCP** and **Pd@ZrCP** revealed considerable reduction in surface area of the pristine framework upon loading palladium nanoparticles from 211 m^2/g to 149 m^2/g (Figure S10 & S12).
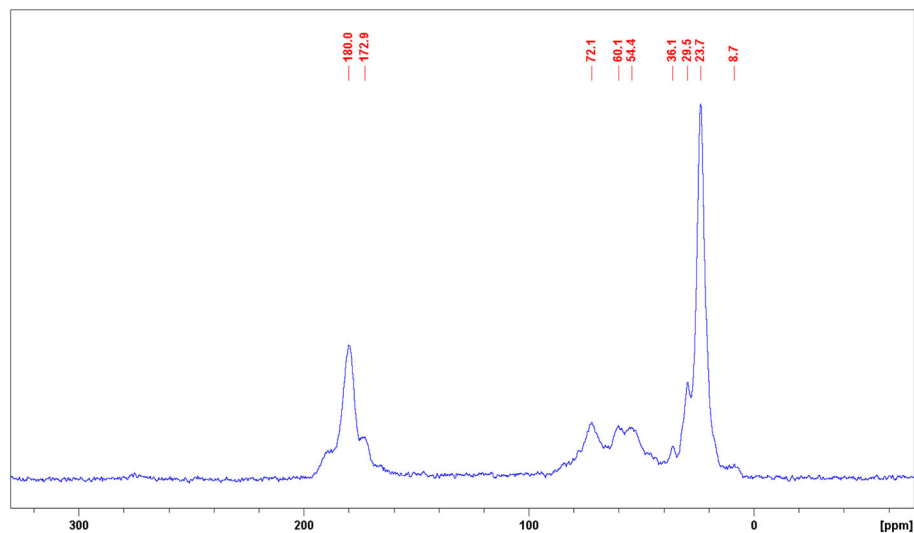
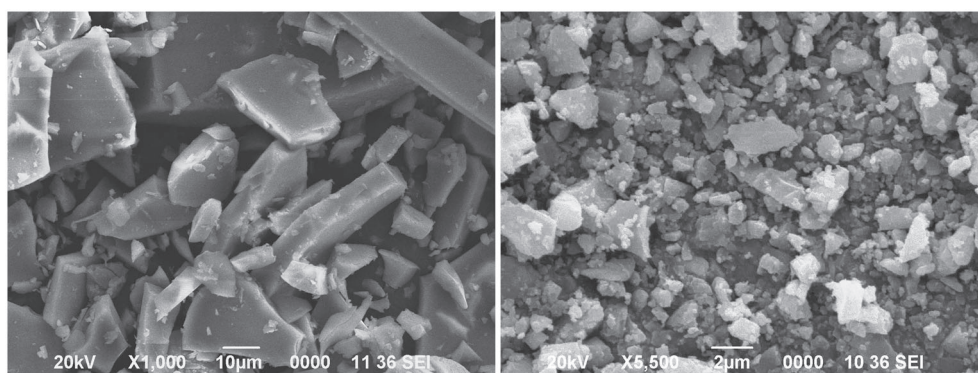**FIGURE 3** ^{13}C MAS NMR spectrum of Pd@ZrCP

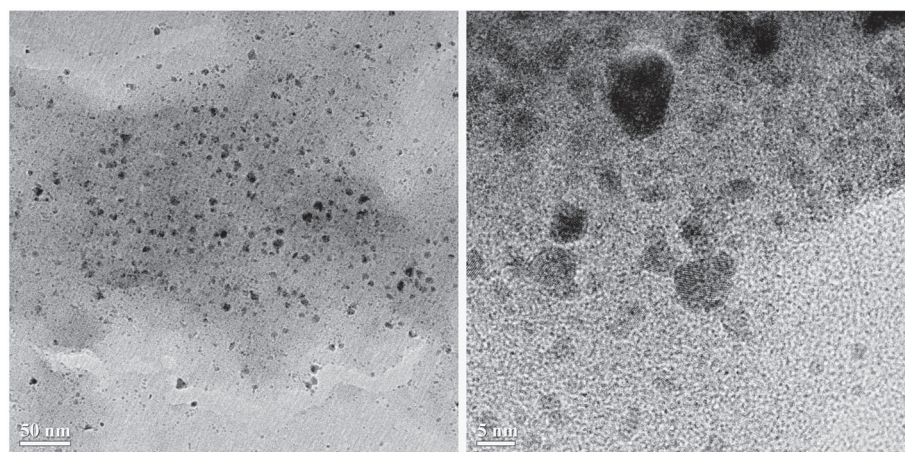**FIGURE 4** SEM images of ZrCP (left) & Pd@ZrCP (right)

FIGURE 5 TEM images of Pd@ZrCP

The influence of loading palladium nanoparticles on the electronic environment of the constituent atoms of the **ZrCP** was further probed by using X-ray photo electron spectroscopy (XPS). The overall XPS spectrum of the pristine framework, **ZrCP** shows characteristic peaks of all the constituent elements present in the framework (Figure S14 and S18). Peaks at 132.8 eV and 133.6 eV corresponds the $2p_{3/2}$ and $2p_{1/2}$ electrons of pentavalent phosphorus (P^{5+}) atom present in **ZrCP** (Figure S16). Upon the incorporation of palladium nanoparticle to the

ZrCP framework, no reasonable shift in the binding energies of $2p_{3/2}$ and $2p_{1/2}$ electrons of P^{5+} are observed as the corresponding peaks appear at 132.5 eV and 133.3 eV (Figure S20), respectively. Furthermore, for the pristine framework, peaks corresponding to $3d_{5/2}$ and $3d_{3/2}$ electrons of tetravalent Zr appear at 182.4 eV and 184.8 eV (Figure S15). Whereas upon loading of palladium to the framework, peaks corresponding to the $3d_{5/2}$ and $3d_{3/2}$ electrons of Zr^{4+} are shifted to a lower binding energies of 181.1 eV and 184.1 eV, respectively (Figure S19). Two peaks observed in the C 1s region of XPS spectrum of **ZrCP** at 284.8 eV and 287.2 eV are characteristic of carbon atoms involved in C-C and C=O bonds, respectively (Figure S17). In case of the palladium loaded framework, peaks corresponding to 1s electron of carbon atoms involved in C-C and C=O bonding are observed at 284.1 eV and 287.1 eV, respectively (Figure S21).

XPS of the **Pd@ZrCP** was investigated further in the Pd(3d) region to explore presence of palladium as well as its electronic state over the framework (Figure 6). Incidentally, binding energy of palladium 3d and binding energy of Zirconium 2p electrons coincide and, therefore, three distinct peaks were observed at 333.2, 340.2 and 346.6 eV. After deconvolution of the parent peaks, peaks at 332.8 eV and 346.6 eV can be, respectively, assigned to $2p_{3/2}$ and $2p_{1/2}$ electrons of tetravalent zirconium. Similarly, peaks at 334.7 eV and 339.9 eV can be assigned to $3d_{5/2}$ and $3d_{3/2}$ electrons of metallic palladium, respectively. However, apart from these peaks an additional set of peaks appeared at binding energies 336.2 eV and 341.5 eV and these indicate the presence of palladium in Pd(II) state. Thus, the XPS spectrum of palladium in **Pd@ZrCP** established the presence of palladium in both Pd(0) and Pd (II) oxidation state while the % proportion of Pd(II) based on peak area is 28%. Presence of unreduced Pd(II) on the surface of metallic palladium
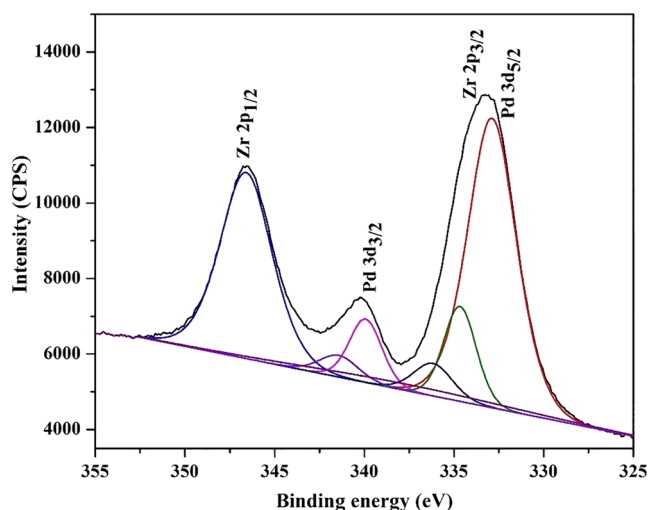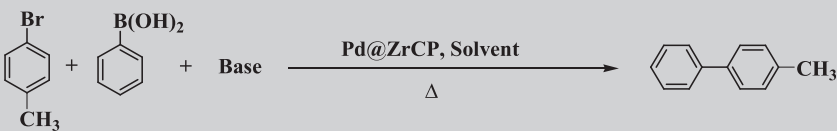
FIGURE 6 XPS spectrum of Pd(3d) region Pd@ZrCP

nanoparticles can be primarily attributed to strong interaction with L-proline. It is pertinent to note here that presence of PdO within the composite has been ruled out as characteristic peak for PdO at $2\theta = 34°$ is not observed in the powder X-ray diffraction pattern of **Pd@ZrCP**.[36] Therefore, presence of Pd^{2+} within the composite has been attributed to the coordination of carboxylate groups of the zirconium carboxyphosphonate framework to the palladium atoms on the surface of the nanoparticles. This hypothesis is also supported by the observation of a strong signal in the ^{13}C MAS NMR of **Pd@ZrCP** at 180.0 ppm which has been attributed to carboxylate groups coordinated to palladium.

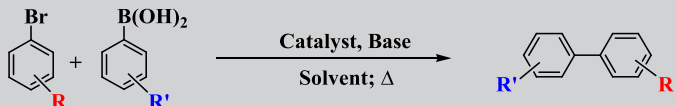# 4 | SUZUKI-MIYAURA CROSS COUPLING REACTION

Palladium has been used extensively as a catalyst in C-C cross coupling reactions. Due to the presence of mixed valent Pd(0)/Pd(II) nanoparticles of average size 5 nm, **Pd@ZrCP** was anticipated to act as a highly active catalyst in C-C coupling reactions. Therefore, the catalytic activity of **Pd@ZrCP** was tested in Suzuki-Miyaura cross coupling reaction of aryl bromides with aryl boronic acids. Initial catalytic investigations carried out by using 4-bromotoluene and phenyl boronic acids as substrates showed satisfactory conversion within a span of 2 minutes. Thereafter, the above reaction was carried out in different conditions to optimize the base, solvent and temperature and the results are summarized in Table 1. By using 0.22 mol% of the catalyst and K_2CO_3 as a base, excellent yields (above 95%) were obtained within 2 mins at 80 °C in aqueous ethanolic medium. However, the reaction did not proceed when only water was used as solvent or in presence of organic base, triethylamine. Nevertheless, under the optimized reaction conditions, the turnover frequency (TOF) of the catalyst, **Pd@ZrCP** in Suzuki-Miyaura cross coupling reaction of 4-bromotoluene and phenyl boronic acids is found to be 1.3×10^4 hr^{-1}, considering the total amount of palladium present. The catalytic efficacy of **Pd@ZrCP** under conventional heating condition is compared with several recently reported heterogeneous catalysts for Suzuki-Miyaura cross coupling reaction (Table 2). **Pd@ZrCP** outperforms all reported state-of-the-art heterogeneous catalyst in terms of reaction completion time as well as TOF as considerably good yields is obtained within a span of two minutes even when 0.22 mol% catalyst is used. Thereafter, cross coupling reaction between several other substituted bromoaryls and *p*-methoxyphenyl boronic acid were investigated by using **Pd@ZrCP** as catalyst under the optimized reaction conditions. The catalyst is found to give satisfactory yields within 2 mins in case of

TABLE 1 Optimization of reaction condition for Pd@ZrCP catalyzed Suzuki-Miyaura reaction

Entry	Solvent	Base	Catalyst	Time (min)	Temp (° C)	Yield (%)
1	$C_2H_5OH{:}H_2O$ (3:1)	K_2CO_3	**Pd@ZrCP**	180	RT	0
2	$C_2H_5OH{:}H_2O$ (3:1)	K_2CO_3	**Pd@ZrCP**	180	40	0
3	$C_2H_5OH{:}H_2O$ (3:1)	K_2CO_3	**Pd@ZrCP**	20	60	23
4	$C_2H_5OH{:}H_2O$ (3:1)	K_2CO_3	**Pd@ZrCP**	2	80	93
5	$C_2H_5OH{:}H_2O$ (3:1)	K_2CO_3	**ZrCP**	90	80	0
6	$C_2H_5OH{:}H_2O$ (2:1)	K_2CO_3	**Pd@ZrCP**	2	80	83
7	$C_2H_5OH{:}H_2O$ (1:1)	K_2CO_3	**Pd@ZrCP**	2	80	78
8	Toluene	K_2CO_3	**Pd@ZrCP**	2	80	trace
9	CH_3OH	K_2CO_3	**Pd@ZrCP**	2	80	78
10	H_2O	K_2CO_3	**Pd@ZrCP**	2	80	0
11	$C_2H_5OH{:}H_2O$ (3:1)	Na_3PO_4	**Pd@ZrCP**	2	80	78
12	$C_2H_5OH{:}H_2O$ (3:1)	NaOH	**Pd@ZrCP**	2	80	81
13	$C_2H_5OH{:} H_2O$ (3:1)	Na_2CO_3	**Pd@ZrCP**	2	80	75
14	$C_2H_5OH{:} H_2O$ (3:1)	Cs_2CO_3	**Pd@ZrCP**	2	80	45
15	$C_2H_5OH{:} H_2O$ (3:1)	NEt_3	**Pd@ZrCP**	2	80	0
16	$C_2H_5OH{:}H_2O$ (3:1)	KOH	**Pd@ZrCP**	2	80	80

Reaction condition: 0.24 mmol phenyl boronic acid; 0.2 mmol 4-bromo toluene; 0.25 mmol base; catalyst 0.5 mg (0.22 mol%)

TABLE 2 Comparison of the present catalyst with some reported catalysts for the Suzuki-Miyaura cross coupling reaction
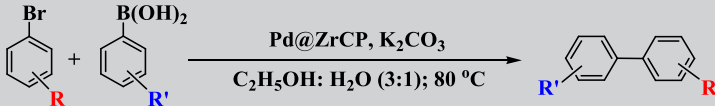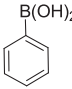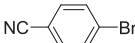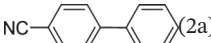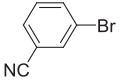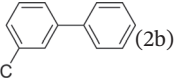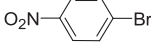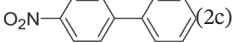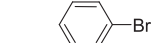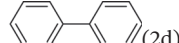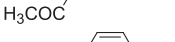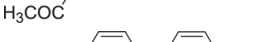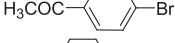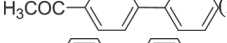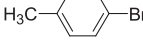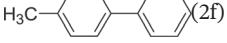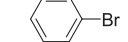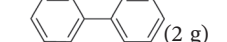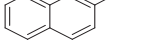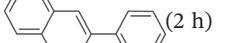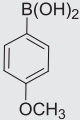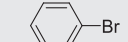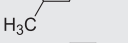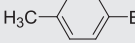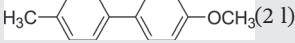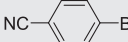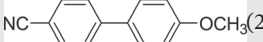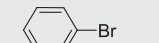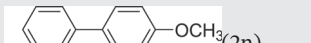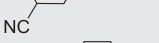
Catalyst	Solvent	Temperature(°C)	Time (Minute)	Yield(%)	Reference
Pd@ZrCP	$EtOH/H_2O$	80	2–10	59–98	This work
$Fe_3Pd_2(OH)_2[PA]_8(H_2O)_4$	DMF	80	20–60	81–100	18
Pd NPs at NHC at ZIF-8	$EtOH/H_2O$	90–120	15–1440	54–99	19
Pd-Fe BN nanosheet	$EtOH/H_2O$	80	30–240	92–100	20
Pd-amino functionalized SiO_2	H_2O	80	30–1440	43–99	21

almost all the substrates tested during this investigation. All the *para* and *meta* substituted aryl bromides with phenyl boronic acid as coupling partner gave good yields up to 98%. However, p–NO_2, p-$COCH_3$, m-$COCH_3$ substituted aryl bromides as well as bulky aryl bromides require slightly longer time of 8–10 mins for completion of the reaction. Furthermore, relatively poor yields were observed in case of all reactions involving p–OCH_3 substituted boronic acid (Table 3).

The recyclability of the catalyst, **Pd@ZrCP** in Suzuki-Miyaura cross coupling reaction was also evaluated

by using p-bromo toluene and phenyl boronic acid as substrates. For this purpose, the heterogeneous catalyst, **Pd@ZrCP** was isolated after each catalytic run and washed with acetone/ethanol and used directly for the next catalytic run. It is observed that the catalyst has excellent recyclability in Suzuki-Miyaura cross coupling reaction as no significant loss of conversion efficiency was observed up to fifth cycle. The recovered catalyst did not show any sign of deactivation as the TOF during fifth catalytic cycle was found to be 1.3×10^4 $hour^{-1}$. The IR spectrum of the catalyst isolated after second and fifth catalytic cycles are

TABLE 3 Suzuki-Miyaura cross coupling reaction with different substrates under optimization condition

Sl no.	Reactant 1	Reactant 2	Product	Time (min)	Yield
	$B(OH)_2$ (phenyl)	NC—C6H4—Br	NC—biphenyl (2a)	2	98%
		NC-substituted bromobenzene	biphenyl (2b)	2	98%
		O_2N—C6H4—Br	O_2N—biphenyl (2c)	10	95%
		H_3COC-substituted bromobenzene	H_3COC—biphenyl (2d)	8	98%
		H_3COC—C6H4—Br	H_3COC—biphenyl (2e)	8	96%
		H_3C—C6H4—Br	H_3C—biphenyl (2f)	2	93%
		H_3C-substituted bromobenzene	H_3C—biphenyl (2 g)	2	95%
		naphthyl bromide	naphthyl phenyl (2 h)	8	80%
		quinoline bromide	quinoline phenyl (2i)	4	89%
		H_3CO—C6H4—Br	H_3CO—biphenyl (2j)	2	87%
	$B(OH)_2$ / OCH_3 (4-methoxyphenyl)	H_3C-substituted bromobenzene	H_3C—biphenyl—OCH_3 (2 k)	2	65%
		H_3C—C6H4—Br	H_3C—biphenyl—OCH_3 (2 l)	2	59%
		NC—C6H4—Br	NC—biphenyl—OCH_3 (2 m)	2	89%
		NC-substituted bromobenzene	NC—biphenyl—OCH_3 (2n)	2	88%
		H_3CO—C6H4—Br	H_3CO—biphenyl—OCH_3 (2o)	2	79%

Reaction condition: 0.24 mmol Aryl boronic acid; 0.2 mmol Aryl halide; 0.25 mmol K_2CO_3; catalyst Pd@ZrCP 0.5 mg (0.22 mol%); solvent: EtOH:H_2O (3:1).

in good agreement with the IR spectrum of the fresh catalyst and all characteristic peaks are observed at nearly identical wave numbers (Figure 7). Furthermore, the powder X-ray diffraction pattern of the catalyst isolated after fifth catalytic run shows a small peak at $2\theta = 39.4°$, characteristic of metallic palladium present in the catalyst and thereby establish the remarkable stability as well as reusability of the present catalyst (Figure S22).

In order to investigate the change in size and morphology of the palladium particles during the course

of Suzuki-Miyaura cross coupling reaction, FE-TEM images of the catalyst isolated after fifth catalytic run were recorded. FE-TEM images clearly reveal that palladium nanoparticles of average size 5 nm are present in the recovered catalyst and the morphology of the particles do not change significantly after 5th catalytic cycle (Figure 8).

Furthermore, leaching test carried out to investigate the possible leaching of palladium from the composite to the reaction solution clearly established that negligible
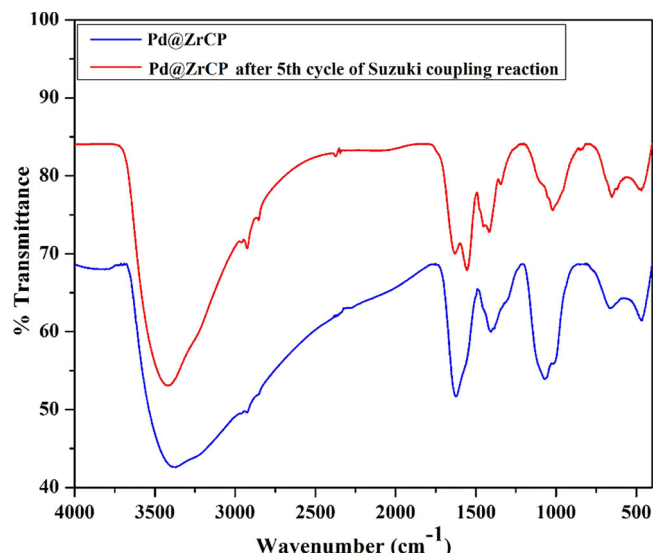
FIGURE 7 FT-IR spectra of catalyst Pd@ZrCP as prepared and after 5th

amount of palladium leached out of the composite, **Pd@ZrCP** even after five consecutive catalytic run. ICP-OES analysis of the organic product isolated after fifth catalytic run did not show any detectable amount of palladium. Furthermore, ICP-OES measurements of the reaction solution showed that the concentration for palladium in reaction solution, both during as well as after completion of the reaction is below the detection limit (50 ppb) of the measurement.

In order to gain insight into the mechanism as well as further establish the heterogeneity of the catalytic species, three phase test has been carried out by using a previously described procedure.[40] For this purpose, 4-bromobenzoylchloride was covalently immobilized on modified silica to prepared a solid supported aryl bromide substrate, $BrPhCONHC_3H_6@SiO_2$. Thereafter, Suzuki-Miyaura cross coupling reaction was carried out by

keeping the soluble reactant $Ph(B(OH)_2)$, insoluble aryl bromide $BrPhCONHC_3H_6@SiO_2$ and the catalyst Pd@ZrCP in three different phases. If the catalytic system remains heterogeneous and no leaching of palladium take place during the reaction, the supported aryl bromide will not participate in cross coupling reaction. A soluble aryl bromide, *p*-bromotoluene was also added to the reaction mixture to ensure presence of an active species and thus mimic the exact reaction condition. During the three phase test, the 4-bromotoluene reacts with phenyl boronic acid to yield 90% cross coupling product within 2 mins. However, the immobilized aryl bromide did not undergo cross coupling reaction which is established by ^1H NMR analysis (Figure S30 & S31) of the immobilized substrate recovered from the three phase test mixture.

Mercury poisoning test was also carried out to investigate the active species present in the catalytic cycle. As reported the catalytic system consist of both Pd(0) and Pd(II) species, the active species that take part in the reaction cycle can be investigated by the mercury poisoning test. The reaction of 4-bromoacetophenone with phenylboronic acid was taken as the model reaction for this test as this substrate takes comparatively longer reaction time than other substrates. The progress of the reaction was monitored by GC–MS, revealed that after 3 minutes 45% conversion occur. Elemental mercury was then added to the reaction mixture and the reaction was further allowed to proceed for another 10 mins. GC–MS analysis of the reaction mixture recovered at this point revealed only 50% conversion and this shows that the active species that present in the catalytic cycle is Pd(0) not Pd(II). However, the small difference in conversion before and after addition of elemental mercury may be attributed to the presence of Pd(II) in the catalytic species as evidenced by XPS analysis discussed above.
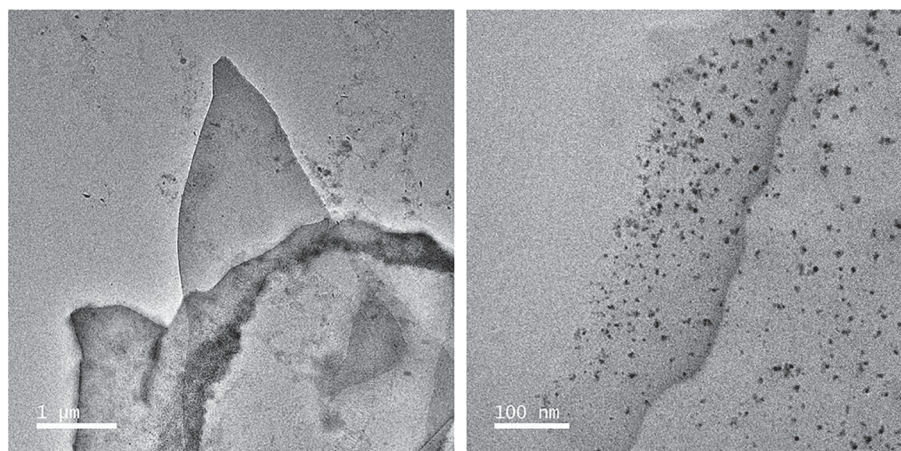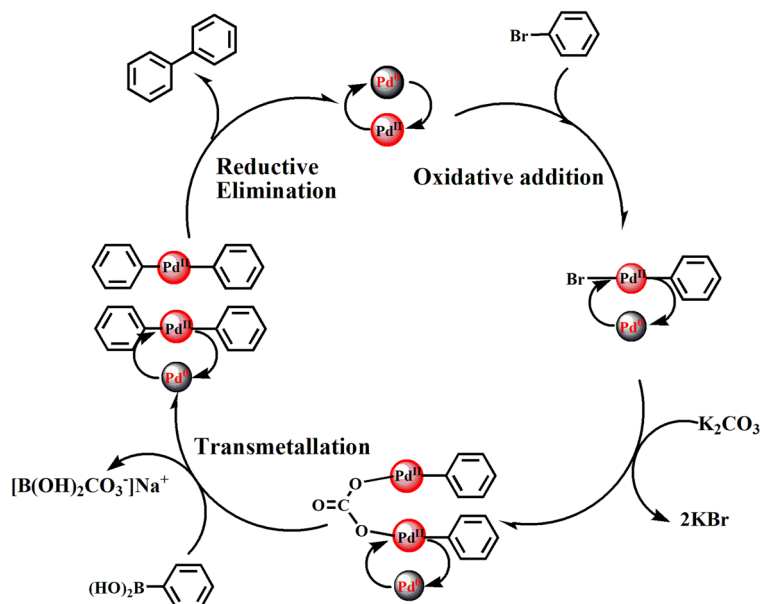

FIGURE 8 TEM images of Pd@ZrCP after 5th catalytic cycle

SCHEME 3 Mechanism of Suzuki-Miyaura cross coupling reaction

It is well established that the Suzuki-Miyaura cross coupling reaction passes through oxidative addition, transmetallation and reductive elimination steps during its catalytic cycle. During the catalytic cycle palladium switches oxidation state from Pd(0) to Pd(II). Palladium leaching test, three phase test and mercury poisoning test suggest heterogenous nature of the present catalyst in Suzuki-Miyaura cross coupling reaction. Based on results, we suggest a plausible mechanism for Suzuki-Miyaura cross coupling reaction catalyzed by Pd@ZrCP (Scheme 3). The remarkably short reaction completion time, recyclability without any loss of catalytic efficacy and resistance to metal leaching of the present catalyst can be attributed to the interaction of surface L-proline groups with the embedded palladium nanoparticles.

5 | CONCLUSION

A remarkably efficient heterogenous catalyst for Suzuki-Miyaura cross coupling reaction has been developed by anchoring surface functionalized palladium nanoparticles onto a layered zirconium carboxyphosphonate based framework. Analytical, spectroscopic, structural, microscopic and textural characterizations were carried out to understand the exact nature of the nanocomposite. Thus, surface functionalization of palladium nanoparticles by L-proline groups dangling on the surface of layered zirconium carboxyphosphonate support is primarily attributed to the highly augmented catalytic efficacy of the present catalytic system. The unprecedentedly short reaction time for completion of the reactions under conventional heating conditions highlights the importance employing mixed valent Pd(0)/Pd(II) catalyst in cross-coupling reactions.

ORCID

Shashank Mishra [iD] https://orcid.org/0000-0003-2846-4221
Nayanmoni Gogoi [iD] https://orcid.org/0000-0001-7398-6200

REFERENCES

[1] F. Zaera, *Catal. Lett.* **2012**, *142*, 501.
[2] A. Corma, *Cat. Rev.-Sci. Eng.* **2004**, *46*, 369.
[3] G. C. Bond, *Chem. Soc. Rev.* **1991**, *20*, 441.
[4] D. W. Goodman, *Chem. Rev.* **1995**, *95*, 523.
[5] G. C. Bond, *Surf. Sci.* **1985**, *156*, 966.
[6] Z. C. Zhang, B. Xu, X. Wang, *Chem. Soc. Rev.* **2014**, *43*, 7870.
[7] A. Molnar, *Chem. Rev.* **2011**, *111*, 2251.
[8] L. Yin, J. Liebscher, *Chem. Rev.* **2007**, *107*, 133.
[9] S. Paul, M. M. Islam, S. M. Islam, *RSC Adv.* **2015**, *5*, 42193.
[10] G. M. Scheuermann, L. Rumi, P. Steurer, W. Bannwarth, R. Mülhaupt, *J. Am. Chem. Soc.* **2009**, *131*, 8262.
[11] N. Erathodiyil, S. Ooi, A. M. Seayad, Y. Han, S. S. Lee, J. Y. Ying, *Chem. – Eur. J.* **2008**, *14*, 3118.
[12] B. J. Gallon, R. W. Kojima, R. B. Kaner, P. L. Diaconescu, *Angew. Chem. Int. Ed.* **2007**, *46*, 7251.

[13] A. Desforges, R. Backov, H. Deleuze, O. Mondain-Monval, *Adv. Funct. Mater.* **2005**, *15*, 1689.

[14] Z. Chen, E. Vorobyeva, S. Mitchell, E. Fako, M. A. Ortuño, N. López, S. M. Collins, P. A. Midgley, S. Richard, G. Vilé, J. Pérez-Ramírez, *Nat. Nanotechnol.* **2018**, *13*, 702.

[15] N. T. S. Phan, M. V. D. Sluys, C. W. Jones, *Adv. Synth. Catal.* **2006**, *348*, 609.

[16] D. Astruc, *Inorg. Chem.* **2007**, *46*, 1884.

[17] C. C. C. Johansson Seechurn, M. O. Kitching, T. J. Colacot, V. Snieckus, *Angew. Chem. Int. Ed.* **2012**, *51*, 5062.

[18] M. Azad, S. Rostamizadeh, F. Nouri, H. Estiri, Y. Fadakar, *Mater. Lett.* **2019**, *236*, 757.

[19] H. Asiabi, Y. Yamini, M. Shamsayei, M. K. Miraki, A. Heydari, *ACS Sustainable Chem. Eng.* **2018**, *6*, 12613.

[20] Q. Fu, Y. Meng, Z. Fang, Q. Hu, L. Xu, W. Gao, X. Huang, Q. Xue, Y. P. Sun, F. Lu, *ACS Appl. Mater. Interfaces* **2017**, *9*, 2469.

[21] S. Shabbir, S. Lee, M. Lim, H. Lee, H. Ko, Y. Lee, H. Rhee, *J. Organomet. Chem.* **2017**, *846*, 296.

[22] A. Turner, P. A. Jaffrès, E. J. MacLean, D. Villemin, V. McKee, G. B. Hix, *Dalton Trans.* **2003**, *7*, 1314.

[23] H. P. Perry, J. Law, J. Zon, A. Clearfield, *Microporous Mesoporous Mater.* **2012**, *149*, 172.

[24] E. A. Clearfield, K. Demadis, *Royal Society of Chemistry*, Cambridge **2011**.

[25] S. Borah, B. Bhattacharyya, J. Deka, A. Borah, A. Devi, D. Deka, S. Mishra, K. Raidongia, N. Gogoi, *Dalton Trans.* **2017**, *46*, 8664.

[26] H. P. Perry, J. Law, J. Zon, *Microporous and Mesoporous Mater.* **2012**, *149*, 172.

[27] S. Borah, S. Mishra, L. Cardenas, N. Gogoi, *Eur. J. Inorg. Chem.* **2018**, *2018*, 751.

[28] T. Y. Ma, Z. Y. Yuan, *Dalton Trans.* **2012**, *39*, 9570.

[29] F. Costantino, R. Vivani, M. Bastianini, L. Ortolani, O. Piermatti, M. Nocchetti, L. Vaccaro, *Chem. Commun.* **2015**, *51*, 15990.

[30] J. Tuteja, H. Choudhary, S. Nishimura, K. Ebitani, *ChemSusChem* **2014**, *7*, 96.

[31] F. Costantino, M. Nocchetti, M. Bastianini, A. Lavacchi, M. Caporali, F. Liguori, *Nano Mater.* **2018**, *1*, 1750.

[32] Y. Tang, Y. Ren, X. Shi, *Inorg. Chem.* **2013**, *52*, 1388.

[33] X. Shi, J. Liu, C. Li, Q. Yang, *Inorg. Chem.* **2007**, *46*, 7944.

[34] S. Calogero, D. Lanari, M. Orrù, O. Piermatti, F. Pizzo, L. Vaccaro, *J. Catal.* **2011**, *282*, 112.

[35] S. Liu, M. Lv, D. Xiao, X. Li, X. Zhou, M. Guo, *Org. Biomol. Chem.* **2014**, *12*, 4511.

[36] G. Zhang, Y. Luan, X. Han, Y. Wang, X. Wen, C. Ding, *Appl. Organomet. Chem.* **2014**, *28*, 332.

[37] E. Nehlig, B. Waggeh, N. Millot, Y. Lalatonne, L. Motte, E. Guenin, *Dalton Trans.* **2015**, *44*, 501.

[38] A. R. Hajipour, E. Boostani, F. Mohammadsaleh, *RSC Adv.* **2015**, *5*, 24742.

[39] X. Shi, J. Yang, Q. Yang, *Eur. J. Inorg. Chem.* **2006**, *2006*, 1936.

[40] C. Baleizaõ, A. Corma, H. Garcıá, A. Leyva, *J. Org. Chem.* **2004**, *69*, 439.

[41] C. M. Hagen, J. A. Widegren, P. M. Maitlis, R. G. Finke, *J. Am. Chem. Soc.* **2005**, *127*, 4423.

[42] R. Silbernagel, C. H. Martin, A. Clearfield, *Inorg. Chem.* **2016**, *55*, 1651.

[43] R. Silbernagel, T. C. Shehee, C. H. Martin, D. T. Hobbs, A. Clearfield, *Chem. Mater.* **2016**, *28*, 2254.

SUPPORTING INFORMATION

Additional supporting information may be found online in the Supporting Information section at the end of the article.